International Journal of Heat and Mass Transfer 52 (2009) 2571–2580

Contents lists available at ScienceDirect

International Journal of Heat and Mass Transfer

journal homepage: www.elsevier.com/locate/ijhmt

An investigation of a high temperature difference natural convection in a finite length channel without Bossinesq assumption

Wu-Shung Fu *, Chung-Gang Li, Chien-Ping Huang, Jieh-Chau Huang

Department of Mechanical Engineering, National Chiao Tung University, 1001 Ta Hsueh Road, Hsinchu 30056, Taiwan, ROC

ARTICLE INFO

Article history:
Received 29 August 2008
Received in revised form 10 January 2009
Available online 9 March 2009

Keywords:
Natural convection
Bossinesq assumption
Preconditioning method
Non-reflection conditions
Roe scheme
Dual-time stepping

ABSTRACT

For expanding industrial applications of a natural convection in a channel under a high temperature difference, a compressible fluid flow is taken into consideration in governing equations instead of renunciation of the Bossinesq assumption. Due to the slowness of the velocity of fluid in the natural convection, the Roe scheme matching methods of preconditioning and dual-time stepping are used to solve the governing equations. In order to resolve reflections induced by acoustic waves at the boundaries of the channel, non-reflection conditions at the boundaries of the channel are derived.

The results show that a more reasonable pressure distribution in the channel is first validated and average Nusselt numbers are expressed in terms of Rayleigh number for a wide range temperature difference.

1. Introduction

A natural convection in an open-ended finite length channel which has always attracted much attention is a very important subject in both academic and industrial researches. The coexistence of the variable density of fluid and slow velocity of flow is the characteristics of the above subject. For avoiding the complexity of solving process caused by the characteristics mentioned above, the Bossinesq assumption in which a factor of the variable density of fluid only affects a buoyancy force is usually adopted when theoretical analysis of the natural convection is executed. As for the boundary conditions at the channel outlet, method of adjustment of the length for satisfying a fully developed flow [1–8] or no pressure difference between the outlet and surroundings is usually used. And the boundary condition at the inlet of the channel, method of matching a mass conservation or based on Bernoulli's equation is proposed.

According to Gray [9], when the temperature difference between the heat and cold sources of the natural convection problem is smaller than 30 K, the results obtained by the Bossinesq assumption are well consistent with the practical situation. However, in many other important natural convection problems, the temperature differences are often higher than several hundred degrees, such as a flow in a chimney, a high temperature drying process and a deposition process in semiconductor manufacturing process. Because of the inapplicability of Bossinesq assumption under the high temperature difference natural convection, the problems mentioned above become very complicated and the related solution methods are seldom proposed. Also, under realistic condition pressure differences between the inside and outside of the inlet and outlet are existent, respectively. Otherwise, the fluid from the outside could not flow into the channel and the fluid in the channel could not be discharged to the outside. These pressure differences would cause acoustic waves induced by the compressibility of fluid to reflect at the inlet and outlet. And when the related numerical calculation is executed, the solutions in the channel are easily polluted by the reflections of the acoustic waves mentioned above which lead the computation processes to be poorly convergent, especially for a low speed compressible flow. Therefore, for analyzing the problem of natural convection in a channel under high temperature difference realistically, in addition to the consideration of the property of viscosity of fluid, the property of compressibility of fluid and the reflection problems at the inlet and outlet should also be considered simultaneously.

Several related numerical methods had been proposed. In an explicit numerical method, the time step due to CFL (Courant–Friedrichs–Levy) condition is limited to an extremely small magnitude, and the convergent condition is difficult to be satisfied. In an implicit numerical method, the stiff situation causes the inefficiency of calculation to occur easily. For overcoming these defects mentioned above, Briley et al. [10] used a preconditioning method to improve the efficiency of calculation for a low Mach number flow, and adopted the implicit numerical method to resolve the convergent problem of Navier–Stokes equation. Turkel [11] developed and applied a preconditioning matrix into problems of

* Corresponding author. Tel.: +886 3 5712121x55110; fax: +886 3 5735065.
E-mail address: wsfu@mail.nctu.edu.tw (W.-S. Fu).

0017-9310/$ - see front matter © 2009 Elsevier Ltd. All rights reserved.
doi:10.1016/j.ijheatmasstransfer.2009.01.012

Nomenclature

g	acceleration of gravity (m/s^2)
k	thermal conductivity (W/mK)
l_0	height of channel (m)
l_1	height from heat surface to top (m)
l_2	height of heat surface (m)
l_3	height from heat surface to bottom (m)
$\dot{m}_x$	mass flow rate (kg/s)
$\overline{\dot{m}}_x$	average mass flow rate (kg/s)
$\underline{Nu}$	local Nusselt numbers
$\overline{Nu}$	average Nusselt number
P	pressure (Pa)
Pr	Prandtl number
R	gas constant (J/kg/K)
Ra	Rayleigh number
t	time (s)
T	temperature (K)
T_c	temperature of surroundings (K)
T_h	temperature of heat surface (K)
u, v	velocities in x and y directions (m/s)
w	width of channel (m)
x, y	cartesian coordinates (m)

Greek symbols

ρ	density (kg/m^3)
μ	viscosity (N s/m^2)
γ	specific heat ratio
β	thermal expansion coefficient (1/K)

compressible and incompressible flows. Choi and Merkel [12] investigated convergent problems induced by the stiff situation and factorization error when an implicit numerical method was used to solve inviscid flow under a low Mach number flow. Moreover, the convergent problem of 0.05 Mach number flow was successfully resolved by using the precondition matrix. Afterward Choi and Merkel [13] proposed an adaptable preconditioning matrix to solve convergent problems of a viscous flow under a low Mach number situation. Roe [14] developed averaged variables method for compressible flow to solve discontinuous phenomenon occurring at a cell interface. This method was widely used in solving compressible flow recently. Weiss and Simth [15] extended the researches of Choi, applied Roe scheme mentioned above with preconditioning method into the solution method of three-dimensional Navier–Stokes equations, and added dual-time stepping to resolve transient states of a low Mach number flow.

Besides, in order to treat boundary conditions at the inlet and outlet of the compressible flow properly, Rudy and Strikwerda [16] proposed a concise non-reflecting boundary condition. Poinsot and Lele [17] developed Navier–Stokes characteristics boundary condition (NSCBC) to resolve problems induced by boundary condition of inlet, outlet and no slip on a wall. The velocities of flow fields investigated by both literature mentioned above were larger than 0.3 Mach number.

Relatively few researchers investigated natural convection problems in which the flow is regarded as a compressible fluid flow. Weiss and Simth [15] adopted the preconditioning method to simulate a natural convection in a two-dimensional concentric circles. The temperatures of inner and outer walls were 2000 K and 1000 K, respectively. The corresponding Rayleigh number was about 4.7×10^4. The results showed that usage of the preconditioning method could reduce 60 times computational time approximately. Paillere et al. [18] used the preconditioning method to calculate a natural convection in a two-dimensional enclosure. The results indicated that heat transfer rates obtained by the small temperature difference were close to these obtained by Bossinesq assumption in spite of high temperatures of heat sources. All the studies mentioned above were in enclosure situations and did not consider the boundary conditions of the inlet and outlet. Yamamoto et al. [19] investigated a natural convection of a circular cylinder set in an external flow. The preconditioning method was used to calculate a compressible flow in a natural convection, and the results had good agreement with experimental results. Because of an external flow, the problems induced by the boundary conditions of the inlet and outlet were not treated. With regard to the study of a high temperature difference, a natural convection of an open-ended finite length channel in which the Bossinesq assumption is not used and the flow is regarded as the compressible fluid flow is seldom investigated.

Therefore, the aim of this study is to investigate a natural convection problem in an open-ended finite length channel numerically. In order to broaden industrial applications, the temperature difference between the heat sources of the high and low temperatures is over several hundred degrees. The Bossinesq assumption is then no longer suitable for this study. For a more realistic simulation, a compressible fluid flow is taken into consideration instead of renunciation of the Bossinesq assumption. Solution methods of Roe, preconditioning and dual-time stepping are combined to resolve the low compressible fluid flow in a transient state. Besides, a modification of the method proposed by Poinsot and Lele [17] is conducted to resolve the reflection problems occurring at both the inlet and outlet of the channel. For improving the efficiency, the calculation process is parallel. The transient developments of pressure, flow and thermal fields are validated. The results obtained by a low temperature difference (<30 K) condition have good agreement with the existing results obtained by using the Bossinesq assumption. And the results of the high temperature difference (>>30 K) conditions show that the Nusselt numbers increase but the increasing rate of Nusselt number decrease with the increment of the temperature difference, and the Nusselt numbers can be expressed in terms of the Rayleigh number. The pressures of the insides of inlet and outlet are smaller and larger than these of the outsides of inlet and outlet, respectively. These results are first validated and more consistent with realistic situations.

2. Physical model

An open-ended finite length channel regarded as a physical model is indicated in Fig. 1. The length and width are l and w, respectively. A heat surface of which the length and temperature are l_2 and T_h, respectively, is installed on the left side of the channel. The distances from the outlet and inlet to the heat surface are l_1 and l_3, respectively. Except the heat surface region, the other regions are adiabatic. The gravity is downward and the temperature and pressure of the surroundings are 298.0592 K and 101,300 Pa, respectively.

For facilitating the analysis, the following assumptions are made.

1. The flow is two-dimensional laminar flow.
2. The fluid is an ideal gas and follows the ideal gas equation of state.

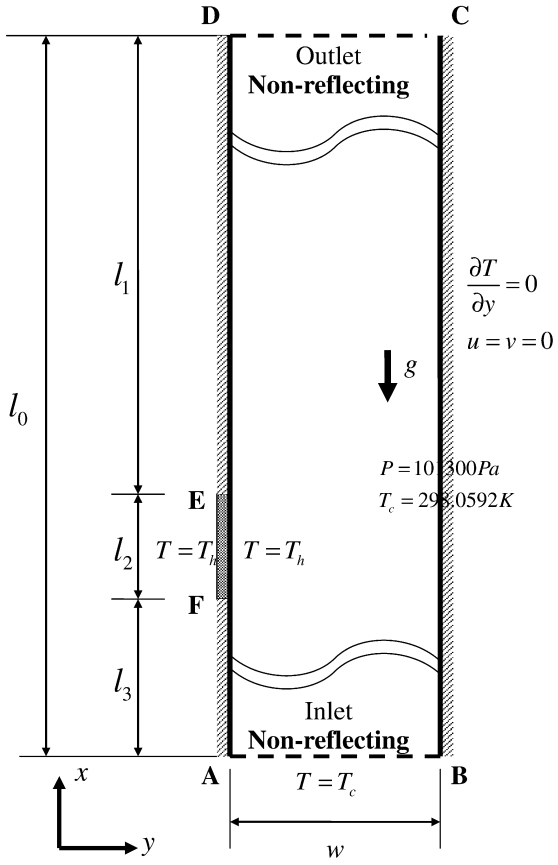

Fig. 1. Physical model.

3. No slip conditions on the surface.
4. Non-reflecting conditions on the inlet and outlet.

The governing equations in which the parameters of viscosity and compressibility of the fluid and gravity are considered simultaneously are shown in the following equations.

$$\frac{\partial U}{\partial t}+\frac{\partial F}{\partial x}+\frac{\partial G}{\partial y}=S \tag{1}$$

$$P=\rho RT \tag{2}$$

The contents of U, F, G and S are indicated as follows.

$$\left.\begin{aligned} U&=\begin{pmatrix}\rho\\ \rho u\\ \rho v\\ \rho E\end{pmatrix}\\ F&=\begin{pmatrix}\rho u\\ \rho u^2+P-\tau_{xx}\\ \rho uv-\tau_{xy}\\ \rho Eu+Pu-k\frac{\partial T}{\partial x}-u\tau_{xx}-v\tau_{xy}\end{pmatrix}\\ G&=\begin{pmatrix}\rho v\\ \rho vu-\tau_{yx}\\ \rho v^2+P-\tau_{yy}\\ \rho Ev+Pv-k\frac{\partial T}{\partial y}-u\tau_{yx}-v\tau_{yy}\end{pmatrix}\\ S&=\begin{pmatrix}0\\ -(\rho-\rho_0)g\\ 0\\ -(\rho-\rho_0)gu\end{pmatrix}\end{aligned}\right\} \tag{3}$$

In which $E=\frac{p}{\rho(\gamma-1)}+\frac{1}{2}(u^2+v^2)$.

The viscosity and thermal conductivity of the fluid are based upon Sutherland's law and shown as follows.

$$\left.\begin{aligned}\mu(T)&=\mu_0\left(\frac{T}{T_0}\right)^{\frac{2}{3}}\frac{T_0+110}{T+110}\\ k(T)&=\frac{\mu(T)\gamma R}{(\gamma-1)Pr}\end{aligned}\right\} \tag{4}$$

where

$\rho_0=1.1842\ \mathrm{kg/m^3}$, $g=9.81\ \mathrm{m/s^2}$,
$\mu_0=1.85\times10^{-5}\ \mathrm{N\,s/m^2}$, $T_0=298.0592\ \mathrm{K}$, $\gamma=1.4$,
$R=287\ \mathrm{J/kg/K}$ and $Pr=0.72$.

3. Numerical method

In a natural convection, the speed of fluid flow is much slower than that of acoustic wave. The Roe method [14] matching preconditioning method are then adopted to resolve the governing equations shown in Eq. (1) which can be derived as the following equation and shown in Eq. (5).

$$\Gamma\frac{\partial U_p}{\partial\tau}+\frac{\partial F}{\partial x}+\frac{\partial G}{\partial y}=S \tag{5}$$

where Γ is a preconditioning matrix proposed by Weiss and Simth [15] and U_p is a primitive form of $[P,u,v,T]^t$.

Discretize Eq. (5), a first order forward difference is used for the time term of $\frac{\partial U_p}{\partial\tau}$, and central differences are used for the terms of $\frac{\partial F}{\partial x}$ and $\frac{\partial G}{\partial y}$. The equation expressed by the difference form is indicated in Eq. (6).

$$\Gamma\frac{U_p^{k+1}-U_p^k}{\Delta\tau}+\frac{1}{\Delta x}\left(F^k_{i+\frac{1}{2}j,k}-F^k_{i-\frac{1}{2}j,k}\right)+\frac{1}{\Delta y}\left(G^k_{ij+\frac{1}{2},k}-G^k_{ij-\frac{1}{2},k}\right)=S^k \tag{6}$$

In Eq. (6) a third order Runge–Kutta method is adopted to resolve U_p^{k+1}, and the detailed processes are indicated as follows.

$$\begin{aligned}U_p^{k+\frac{1}{3}}&=U_p^k+\Gamma^{-1}R^k\\ U_p^{k+\frac{2}{3}}&=\frac{3}{4}U_p^k+\frac{1}{4}U_p^{k+\frac{1}{3}}+\frac{1}{4}\Gamma^{-1}R^{k+\frac{1}{3}}\\ U_p^{k+1}&=\frac{1}{3}U_p^k+\frac{2}{3}U_p^{k+\frac{2}{3}}+\frac{2}{3}\Gamma^{-1}R^{k+\frac{2}{3}}\end{aligned} \tag{7}$$

where

$$R^{\Phi}=-\Delta\tau\left[\frac{1}{\Delta x}\left(F^{\Phi}_{i+\frac{1}{2}j,k}-F^{\Phi}_{i-\frac{1}{2}j,k}\right)+\frac{1}{\Delta y}\left(G^{\Phi}_{ij+\frac{1}{2},k}-G^{\Phi}_{ij-\frac{1}{2},k}\right)\right]+S^{\Phi},$$

$$\Phi=k,k+\frac{1}{3},k+\frac{2}{3}.$$

Additionally, the method of dual-time stepping is added to calculate the transient state of the physical model. The derived equation is shown in Eq. (8).

$$\Gamma\frac{\partial U_p}{\partial\tau}+\frac{\partial U}{\partial t}+\frac{\partial F}{\partial x}+\frac{\partial G}{\partial y}=S \tag{8}$$

Discretize Eq. (8) and the related difference form is indicated in Eq. (9).

$$\begin{aligned}\Gamma\frac{U_p^{k+1}-U_p^k}{\Delta\tau}+\frac{3U^{k+1}-4U^n+U^{n-1}}{2\Delta t}+\frac{1}{\Delta x}\left(F^k_{i+\frac{1}{2}j,k}-F^k_{i-\frac{1}{2}j,k}\right)\\ +\frac{1}{\Delta y}\left(G^k_{ij+\frac{1}{2},k}-G^k_{ij-\frac{1}{2},k}\right)=S^k\end{aligned} \tag{9}$$

where k is an iteration number of the artificial time step, and n is a time step of the real time. When the term of the artificial time $\frac{\partial U_p}{\partial\tau}$ is convergent to $\varepsilon(=10^{-3})$, the magnitude of the $(k+1)$th iteration of the artificial time term is equivalent to the magnitude of the

$(n+1)$th time step of the real time, and Eq. (9) automatically transfers to the Navier–Stokes equation including the time term.

The term of U^{k+1} can be linearized by the following term.

$$U^{k+1} = U^k + M(U_p^{k+1} - U_p^k) \tag{10}$$

In which $M = \frac{\partial U}{\partial U_p}$.Substitute Eq. (10) into Eqs. (9) and (11) is obtained.

$$\left[\Gamma + M\frac{3\Delta\tau}{2\Delta t}\right](U_p^{k+1} - U_p^k) = R^k \tag{11}$$

where

$$R^k = -\left(\frac{3U^k - 4U^n + U^{n-1}}{2\Delta t}\right) - \left[\frac{1}{\Delta x}\left(F^k_{i+\frac{1}{2},j,k} - F^k_{i-\frac{1}{2},j,k}\right) + \frac{1}{\Delta y}\left(G^k_{i,j+\frac{1}{2},k} - G^k_{i,j-\frac{1}{2},k}\right)\right] + S^k$$

Divide both sides of Eq. (11) by $\left[\Gamma + M\frac{3\Delta\tau}{2\Delta t}\right]$, and Eq. (12) is derived.

$$U_p^{k+1} = U_p^k + \left[\Gamma + M\frac{3\Delta\tau}{2\Delta t}\right]^{-1} R^k \tag{12}$$

Similarly, the magnitude of U_p^{k+1} is obtained by usage of the third order Runge–Kutta method. In the calculating processes of Eqs. (11) and (12), the contents of the term of F are divided into two parts of inviscid term $F_{inviscid}$ and viscous term $F_{viscous}$.

$$F_{inviscid} = \begin{pmatrix} \rho u \\ \rho u^2 + P \\ \rho uv \\ \rho Eu + Pu \end{pmatrix} \tag{13}$$

$$F_{viscous} = \begin{pmatrix} 0 \\ -\tau_{xx} \\ -\tau_{xy} \\ -k\frac{\partial T}{\partial x} - u\tau_{xx} - v\tau_{xy} \end{pmatrix} \tag{14}$$

Utilize methods of the Roe [14] and preconditioning to calculate the magnitude of $F_{inviscid}$ at the position of $(i+\frac{1}{2})$ between the cells for low Mach number condition.

$$F_{inviscid,i+\frac{1}{2}} = \frac{1}{2}(F_R + F_L) - \frac{1}{2}\{|\Gamma^{-1}A_p|\Delta U_P\} \tag{15}$$

where $A_p = \left(\frac{\partial F}{\partial U_p}\right)$ is a flux jacobian.

The magnitude of ΔU_P in Eq. (15) is obtained by the third order precision of MUSCL (Monotone Upwind-centered Schemes for Conservation Laws) method.

$$\Delta U_P = u^L_{i+1/2} - u^R_{i+1/2} \tag{16}$$

$$u^L_{i+1/2} = u_i + 1/2\Delta u^L_{i+1/2} \tag{17}$$

$$u^R_{i+1/2} = u_i - 1/2\Delta u^R_{i+1/2} \tag{18}$$

In which

$$\Delta u^L_{i+1/2} = \frac{2}{3}(u_{i+1} - u_i) + \frac{1}{3}(u_i - u_{i-1}) \tag{19}$$

$$\Delta u^R_{i+1/2} = \frac{2}{3}(u_{i+1} - u_i) + \frac{1}{3}(u_{i+2} - u_{i+1}) \tag{20}$$

The method for calculating the magnitude of $F_{inviscid}$ was proposed by Stokes.

$$\tau_{xx} = -\frac{2}{3}\mu\left(\frac{\partial u}{\partial x} + \frac{\partial v}{\partial y}\right) + 2\mu\frac{\partial u}{\partial x} \tag{21}$$

$$\tau_{xy} = \mu\left(\frac{\partial u}{\partial y} + \frac{\partial v}{\partial x}\right) \tag{22}$$

The forth central difference is adopted to calculate the magnitudes of the difference terms in Eqs. (21) and (22).

$$\frac{\partial u}{\partial x} = \frac{u_{i-2} - 8u_{i-1} + 8u_{i+1} - u_{i+2}}{12\Delta x} + o(\Delta x^4) \tag{23}$$

On the adiabatic surface, the boundary conditions are

$$\begin{aligned} P(i,0) &= P(i,1) \\ u(i,0) &= -u(i,1) \\ v(i,0) &= -v(i,1) \\ T(i,0) &= T(i,1) \end{aligned} \tag{24}$$

On the heat surface, the boundary conditions are

$$\begin{aligned} P(i,0) &= P(i,1) \\ u(i,0) &= -u(i,1) \\ v(i,0) &= -v(i,1) \\ T(i,0) &= 2T_h - T(i,1) \end{aligned} \tag{25}$$

0 is ghost cell and 1 is the first grid from the wall, the positions of 0 and 1 are shown in Fig. 2.

As for the boundary conditions of the outlet and inlet, in order to avoid the flow in the channel polluted by the reflection of acoustic waves mentioned above, the non-reflecting boundary conditions are then necessarily used at the outlet and inlet, respectively.

In a high speed compressible flow condition, the method of LODI (local one-dimensional inviscid relations) proposed by Poinsot and Lele [17] was suitably adopted for determining the non-reflecting boundary conditions at the outlet and inlet. However, a preconditioning matrix is not necessary in the above method that causes this method to be not appropriately adopted for determining the non-reflecting boundary conditions at the outlet and inlet under a low speed compressible flow. As a result, modification of the method mentioned above is necessary for resolving the outlet and inlet boundary conditions under an extremely low speed compressible flow. The variations of densities of fluids are small near the regions of the outlet and inlet, respectively. The term of S indicated in Eq. (1) can be neglected. Then a flow field near the regions of outlet and inlet can be approximately described by the following one-dimensional Navier–Stokes equation.

$$\Gamma\frac{\partial U_p}{\partial \tau} + \frac{\partial F}{\partial x} = 0 \tag{26}$$

Multiply Γ^{-1} on the left side of Eq. (26) in order to transform the term of $\frac{\partial F}{\partial x}$ to be a primitive form.

$$\frac{\partial U_p}{\partial \tau} + \Gamma^{-1}\frac{\partial F}{\partial x} = 0 \tag{27}$$

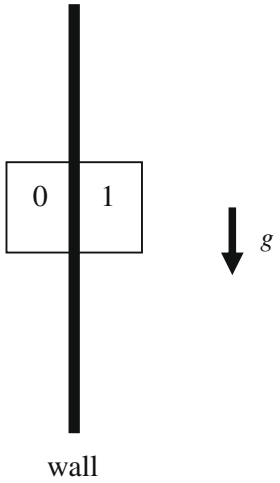

Fig. 2. The grids distribution on the wall.

Transform the term of $\Gamma^{-1}\frac{\partial F}{\partial x}$

$$\Gamma^{-1}\frac{\partial F}{\partial x}=\Gamma^{-1}\frac{\partial F}{\partial U_p}\frac{\partial U_p}{\partial x}=\Gamma^{-1}A_p\frac{\partial U_p}{\partial x} \tag{28}$$

Substitute Eq. (28) into Eq. (26), obtain the following equation based on the primitive form.

$$\frac{\partial U_p}{\partial \tau}+\Gamma^{-1}A_p\frac{\partial U_p}{\partial x}=0 \tag{29}$$

A similar transformation of the term of $\Gamma^{-1}A_p$ is executed to obtain the characteristic velocities of the outlet and inlet.

$$\Gamma^{-1}A_p=K\lambda K^{-1} \tag{30}$$

where K is an eigenvector, λ are eigenvalues of the term of $\Gamma^{-1}A_p$, as well λ are characteristic velocities at the outlet and inlet. According to Dennis et al. [20], transform the orders of u (original flow speed) and c (original acoustic wave speed) to become the similar orders of u' (modified flow speed) and c' (modified acoustic wave speed), and the following equation is obtained.

$$\lambda=\begin{pmatrix}\lambda_1\\ \lambda_2\\ \lambda_3\\ \lambda_4\end{pmatrix}=\begin{pmatrix}u\\ u\\ u'+c'\\ u'-c'\end{pmatrix} \tag{31}$$

where $u'=\frac{(\beta+1)u}{2}$ and $c'=\frac{\sqrt{u^2(\beta-1)^2+4\beta c^2}}{2}$.

Let

$$L=\lambda K^{-1}\frac{\partial U_p}{\partial x} \tag{32}$$

The contents of the term of L are

$$L=\begin{pmatrix}L_1\\ L_2\\ L_3\\ L_4\end{pmatrix}=\begin{pmatrix}u\frac{\partial T}{\partial x}+\frac{1}{\rho\kappa}\left(\frac{\partial P}{\partial x}-\kappa\frac{\partial P}{\partial x}\right)\\ -u\frac{\partial v}{\partial x}\\ (u'+c')\left[\frac{\partial P}{\partial x}-\rho(u'-c'-u)\frac{\partial u}{\partial x}\right]\\ (u'-c')\left[\frac{\partial P}{\partial x}-\rho(u'+c'-u)\frac{\partial u}{\partial x}\right]\end{pmatrix} \tag{33}$$

The physical meaning of the term of L is the magnitude of wave amplitude with time variation.

Substitute Eq. (32) into Eq. (29).

$$\frac{\partial U_p}{\partial \tau}+KL=0 \tag{34}$$

Derive Eq. (34), the following equations which describe the pressure and velocities vertically to stride over the outlet and inlet are obtained, respectively.

$$\frac{\partial P}{\partial \tau}+\frac{1}{2c'}[L_3(u'+c'-u)-L_4(u'-c'-u)]=0 \tag{35}$$

$$\frac{\partial u}{\partial \tau}+\frac{1}{2\rho c'}(L_3-L_4)=0 \tag{36}$$

At the outlet, the magnitude of wave amplitude reflecting from the outlet back to the channel varying with time is L_4. For avoiding the effect of the pollution induced by the reflection of the acoustic wave on the computational domain in the channel, the magnitude of L_4 is conveniently assigned to be 0. Then Eqs. (35) and (36) become Eqs. (37) and (38), respectively.

$$\frac{\partial P}{\partial \tau}+\frac{1}{2c'}[L_3(u'+c'-u)]=0 \tag{37}$$

$$\frac{\partial u}{\partial \tau}+\frac{1}{2\rho c'}L_3=0 \tag{38}$$

From Eq. (38)

$$L_3=-2\rho c'\frac{\partial u}{\partial \tau} \tag{39}$$

Substitute Eq. (39) into Eqs. (37) and (40) is obtained.

$$\frac{\partial P}{\partial \tau}-\rho(u'+c'-u)\frac{\partial u}{\partial \tau}=0 \tag{40}$$

Eq. (40) means the variations of pressure and velocity with time near the outlet. As a result, discretize Eq. (40), and the pressure boundary condition at the outlet can be obtained.

$$P_{out}^{k+1}=P^k-\rho(u'+c'-u)(u^{k+1}-u^k) \tag{41}$$

where k is an iteration number and the same iteration number in Eq. (9).

For the same reason, at the inlet the magnitude of L_3 is also conveniently assigned to be 0. Eqs. (35) and (36) become the following equations, respectively.

$$\frac{\partial P}{\partial \tau}-\frac{1}{2c'}[L_4(u'-c'-u)]=0 \tag{42}$$

$$\frac{\partial u}{\partial \tau}-\frac{1}{2\rho c'}L_4=0 \tag{43}$$

The equation indicating the variations of pressure and velocity with time near the inlet is shown as follows.

$$\frac{\partial P}{\partial \tau}-\rho(u'-c'-u)\frac{\partial u}{\partial \tau}=0 \tag{44}$$

Discretize Eq. (44) and obtain the pressure boundary condition at the inlet.

$$P_{inlet}^{k+1}=P^k-\rho(u'-c'-u)(u^{k+1}-u^k) \tag{45}$$

A procedure calculating the equations mentioned above is briefly described as follows.

(1) Assign the initial conditions of the pressure, velocity and temperature in the channel.
(2) Use Eqs. (41) and (45) to calculate the pressures of the outlet and inlet.
(3) Use MUSCL method calculating Eqs. (17), (18) and (16) to obtain the magnitudes of $u_{i+1/2}^L, u_{i+1/2}^R$ and ΔU_P.
(4) Substitute the magnitude of ΔU_P into Eq. (15) and use Roe method to calculate the magnitude of the term of $F_{inviscid}$.
(5) Calculate Eq. (23) to obtain the magnitudes of viscous terms and substitute into Eq. (14).
(6) Calculate Eq. (7) to obtain a new magnitude of U_p^{k+1}.
(7) Under a steady state, examine the convergence of the iterational computation of U_p^{k+1}. Repeat the processes from (2)–(6) if the convergent condition is not satisfied.

Under a transient state, calculate Eq. (9) and examine the convergence of the iterational computation of the $\frac{\partial U_p}{\partial \tau}$. When the convergent condition is satisfied, the magnitude of U_p^{k+1} will be regarded as that of U_p of the $(n+1)$th time step and the process proceeds to next time step. In order to economize the consumption of computing time, parallel computations are executed by eight processors.

4. Results and discussion

The working fluid used in this study is air and the Prandtl number is 0.72. The pressure and temperature of surroundings are 101,300 Pa and 298.0592 K, respectively. Two kinds of grid distributions are used to examine the adoptable grid distribution used in this study. The results of distributions of u, v and T parallel to the y axis at the center of the heat surface are shown in Fig. 3. The deviations of both the results obtained by the two kinds of grid distributions are slight, the uniform grid distribution of 500×40 is used.

A natural convection in an enclosure of which the temperatures of two heat sources are 606 K and 594 K, respectively, was

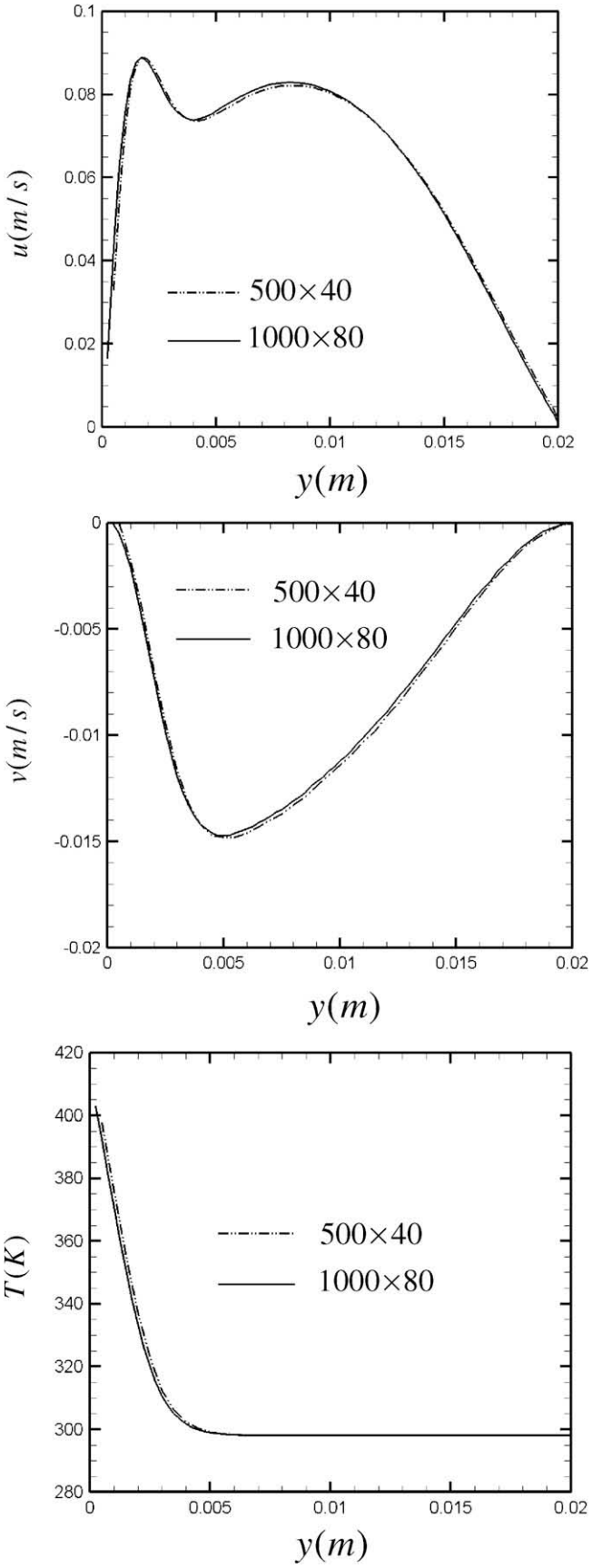

Fig. 3. Comparisons of velocity and temperature profiles parallel to y axis at the center of the heat surface ($Ra = 10^4$).

investigated by Paillere et al. [18]. The compressibility and viscosity of the working fluid were considered, and the definitions of local Nusselt and Rayleigh numbers are separately indicated as follows.

$$Nu = \frac{L}{k_0(T_h - T_c)}\left[k(T)\frac{\partial T}{\partial y}\right]_w \tag{46}$$

$$Ra = Pr\frac{g\rho_0^2(T_h - T_c)L^3}{T_0\mu(T)^2} \tag{47}$$

The local Nusselt numbers of both the results shown in Fig. 4 have good agreement. The numerical method of this study is correct.

According to Gray [9], when the temperature difference of natural convection between two heat sources is smaller than 30 K, the results based on the Bossinesq assumption are well consistent with experimental results. In order to examine the suitability of this study under a low temperature difference, the temperature difference of two heat sources of 10 K is assigned and the computational method developed by this study in which the Bossinesq assumption is not yielded is used to investigate the same subject investigated by Churchill and Chu [21] and Fu and Huang [4]. The definitions of the average Nusselt number $\overline{Nu}$ and Rayleigh number Ra are shown as follows, respectively.

$$\overline{Nu} = \int_{l_2}\frac{l_2}{(T_h - T_c)}\left[\frac{\partial T}{\partial y}\right]_w dx \Big/ l_2 \tag{48}$$

$$Ra = Pr\frac{g\rho_0^2\beta(T_h - T_c)l_2^3}{\mu^2} \tag{49}$$

where β is thermal expansion coefficient.

Use the same physical model of Fu and Huang [4] and Churchill and Chu [21], and the magnitudes of the characteristic length used in Eq. (49) are adjusted to match the same Rayleigh numbers adopted in [21,4]. The results are shown in Fig. 5, and all the results are in good agreement. The results of this study under a low temperature difference are reasonable.

In Fig. 6, the variations of streamlines, pressure contour and thermal field with time under $Ra = 10^4$ are indicated. The initial conditions of the temperature and pressure of the fluid in the channel are the same as these of the surroundings. As time $t > 0$, the temperature of the heat surface is raised to T_h. The conditions of $l_1/l_2 = 19$, $l_0/l_2 = 25$, $w/l_2 = 2$ and $\Delta T = T_h - T_c = 110$ K are assigned. Shown in Fig. 6(1), the time t is 0.005 s, heat energy transferred to the fluid from the heat surface is mainly dependent on a heat

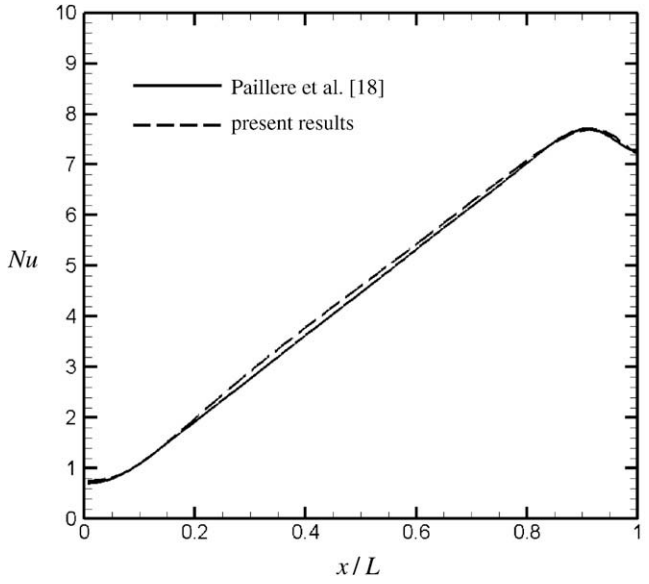

Fig. 4. The distributions of local Nusselt number on the wall of high tempreature.

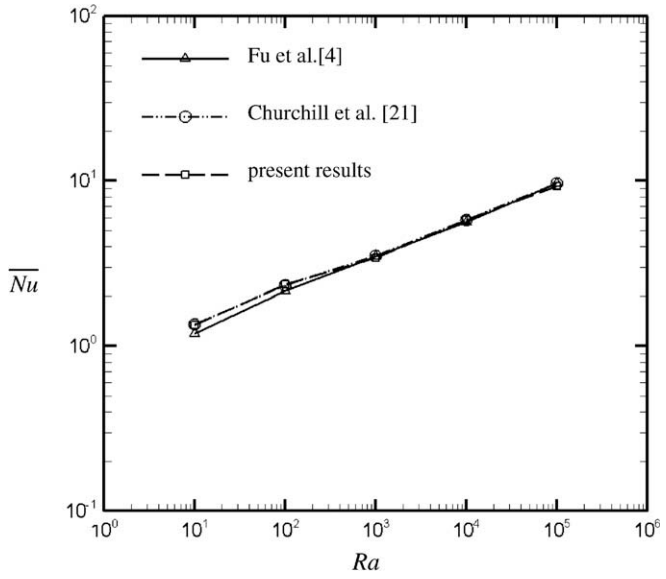

Fig. 5. Comparisons with the results of the present study and other papers.

conduction mode indicated in Fig. 6(1)c. Because of the absorption of heat energy, the densities of the fluids become light and the volume of the fluid shown in Fig. 6(1)b is expanded. Consequently, some fluids shown in Fig. 6(1)a are exhausted to the outsides of the outlet and inlet, respectively. The magnitudes of pressure shown in the figure are the pressure differences as well as the gage pressures between the static pressures of the fluids and the pressure of surroundings. As the time t increases to 0.02 s, the influence of buoyancy force which leads the fluids to flow upwards starts to appear. Below the heat surface region the directions of the fluid flows change from downward to upward shown in Fig. 6(2)a, and accompanying with the upward flow mentioned above a circulation zone is formed near the heat surface region which causes a low pressure zone to appear shown in Fig. 6(2)b. Simultaneously the thermal field shown in Fig. 6(2)c extends upwards.

As the time is 0.05 s, at the inlet the fluid flows are affected by the buoyancy force, and the fluids are sucked from the outside of the inlet and flow into the channel indicated in Fig. 6(3)a. The circulation zone is enlarged and raised gradually. Accompanying with the rising of circulation zone the low pressure zone is also raised. And the plus and minus pressure difference zones are formed above and below the lowest pressure zone, respectively. Meanwhile the thermal field extends further. As the time equals to 0.1 s, the influence of buoyancy force increases continuously. In Fig. 6(4)a the flow structure in which the fluids are sucked from the outside of the inlet and spat to the outside of the outlet is approximately formed. And the large circulation zone shown in the above figure is divided into two small circulation zones. The variations of the magnitudes of pressure difference from the inlet to the outlet are from minus to plus continuously.

Finally, the development of flow structure finishes at $t = 1$ s indicated in Fig. 6(5)a. The heat surface is installed on the left side of the channel which causes the fluids induced by the natural convection mainly to flow along the left side and to form a large circulation zone on the right side. The variations of the magnitudes of pressure difference from the inlet to the outlet are smooth. At the inlet, the magnitude of pressure difference is minus which means the fluids to be sucked from the outside of the inlet and to flow into the channel. At the outlet, the magnitude of pressure difference is plus which indicates the fluids to be discharged to the outside of the outlet naturally. Shown in [6], under the usage of Boussinesq assumption condition the magnitude of pressure difference at the outlet ceased to be negative which means the pressure at the outlet to be equivalent to that of the surroundings. It is arguable that under no pressure difference condition, the fluids can flow from the inside to the outside of the outlet.

In Fig. 7, the velocity profile obtained by this work at the inlet under a steady state ($t = 1$ s) is indicated. The velocity profile is almost a uniform flow which was validated by the experimental results [6]. An assumption of a uniform flow at the inlet always made in the previous studies is reasonable.

Shown in Fig. 8, comparisons of the average mass flow rate of the channel $\bar{\dot{m}}_x$ with the mass flow rate at each cross section $\dot{m}_x$ of the channel are indicated. The definitions of $\bar{\dot{m}}_x$ and $\dot{m}_x$ are expressed as follows, respectively.

$$\bar{\dot{m}}_x = \int_0^{l_0}\int_0^{w} \rho u\, dy\, dx / l_0 \tag{50}$$

$$\dot{m}_x = \int_0^{w} \rho u\, dy \tag{51}$$

Shown in the Fig. 8, the maximum derivation between $\bar{\dot{m}}_x$ and $\dot{m}_x$ is about 3%. According to the results of Xu et al. [23] and Lenormand et al. [24], in a duct flow through the influence of the friction induced by shear stress and the dissipation induced by numerical calculation, the conservation of mass flow rate can not be held completely. The mass flow rate will decrease gradually from inlet to outlet, and this phenomenon is more remarkable in a compressibly viscous flow. So the results indicated in Fig. 8 are reasonable and accurate.

In Fig. 9, comparisons of the local Nusselt numbers along the heated surface for different Rayleigh numbers in which only the parameter of temperature difference is different are shown. Naturally the larger the temperature difference is, the larger the Nusselt number is obtained. However the increasing rate of the local Nusselt number becomes small as the temperature difference increases.

The average Nusselt number $\overline{Nu}_{l_2}$ which is slightly different from that defined in Eq. (48) is defined as follows.

$$\overline{Nu}_{l_2} = \int_{l_2} \frac{l_2}{k_0(T_h - T_c)} \left[k(T)\frac{\partial T}{\partial y}\right]_w dx \Big/ l_2 \tag{52}$$

A correlation equation based on the numerical results of this work is derived and shown in Eq. (53).

$$\overline{Nu}_{l_2} = (1/1.26) \times Ra^{\frac{1}{4.69}} \tag{53}$$

The relationships between the numerical results and correlation equation are indicated in Fig. 10. The equation is adoptable for a wide temperature differences range that is useful for industrial applications.

Usually a fully developed flow is used as a boundary condition of an outlet when a study of incompressible channel flow is executed. In order to match the boundary condition of fully developed flow, the length of the channel should be elongated. The condition of fully developed flow at the outlet is not necessary in this study. The effect of l_1 which is measured from the heat surface to the outlet and indicated in Fig. 1 on the average Nusselt number is investigated and shown in Fig. 11. The corresponding correlation equation is indicated in Eq. (54).

$$\overline{Nu}_{l_2} = [\log(l_1/l_2 + 1)]^{0.28} + 4.49 \tag{54}$$

Since the walls of the channel are insulated except the heat surface and the temperature and pressure of the surroundings are 298.0592 K and 101300 Pa, respectively. The temperatures of the fluids heated by the heat surface in the channel are higher than that of the surroundings which cause the densities of fluids in the channel to be less than that of the surroundings. Consequently, the buoyancy force always exists in the whole channel, so the longer the channel is, the influence of the buoyancy force on the fluid flow

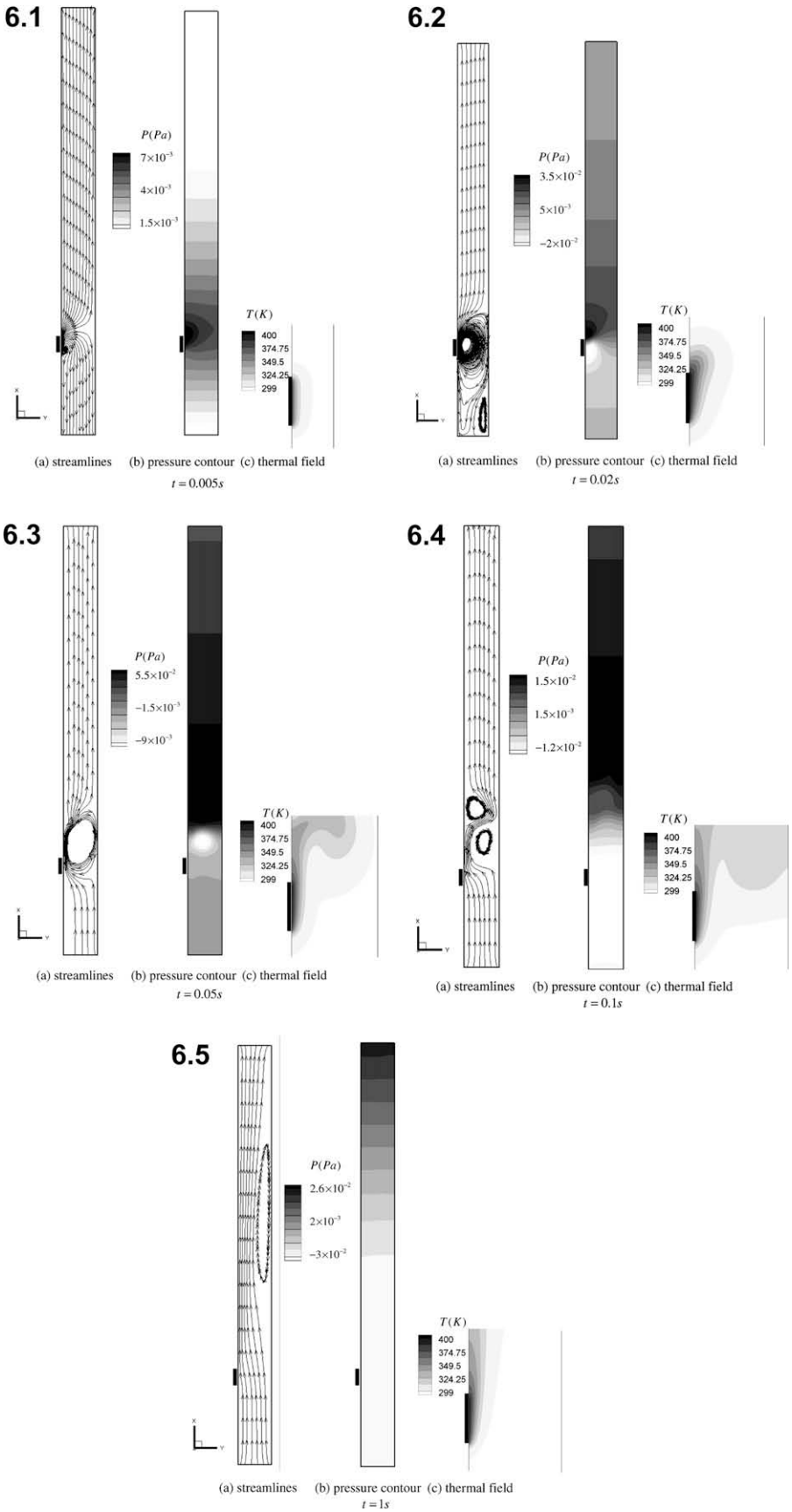

Fig. 6. (1) The variants of streamlines, pressure contour and thermal field with t time under ($Ra = 10^4$) ($l_1/l_2 = 19$). (2) The variants of streamlines, pressure contour and thermal field with time under ($Ra = 10^4$) ($l_1/l_2 = 19$). (3) The variants of streamlines, pressure contour and thermal field with time under ($Ra = 10^4$) ($l_1/l_2 = 19$). (4) The variants of streamlines, pressure contour and thermal field with time under ($Ra = 10^4$) ($l_1/l_2 = 19$). (5) The variants of streamlines, pressure contour and thermal field with time under ($Ra = 10^4$) ($l_1/l_2 = 19$).

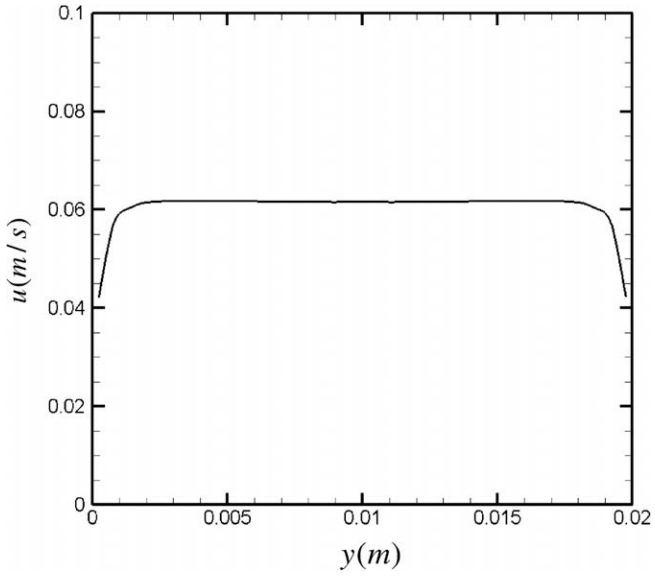

Fig. 7. The velocity profile at the inlet at $t = 1$ s condition ($l_1/l_2 = 19$).

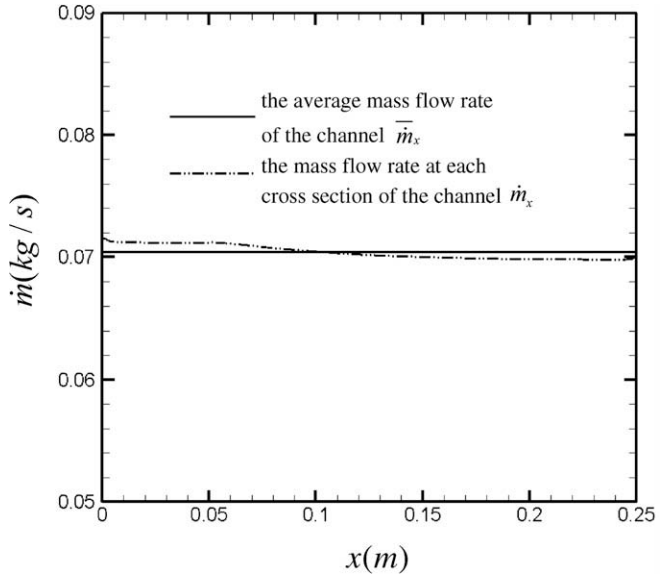

Fig. 8. Comparisons of the average mass flow rate of the channel with the mass flow rate at each cross section of the channel ($l_1/l_2 = 19$).

becomes more apparent. Accompanying with the above phenomena, the average Nusselt number increases with the increment of the length of the channel shown in Fig. 11. The increasing rate of the average Nusselt number decreases as the ratio of $l_1/(l_1 + l_1)$ is over 10. However, when the conditions of temperature and pressure of the surroundings are different from these of the study, the results of this study will be varied.

5. Conclusions

For expanding industrial applications, a compressible fluid flow is considered instead of renunciation of the Bossinesq assumption in an investigation of a natural convection in a channel. Solution methods of Roe scheme, preconditioning and dual-time stepping are combined to solve governing equations and non-reflecting conditions are adopted at the inlet and outlet. Based on the results, the following can be concluded:

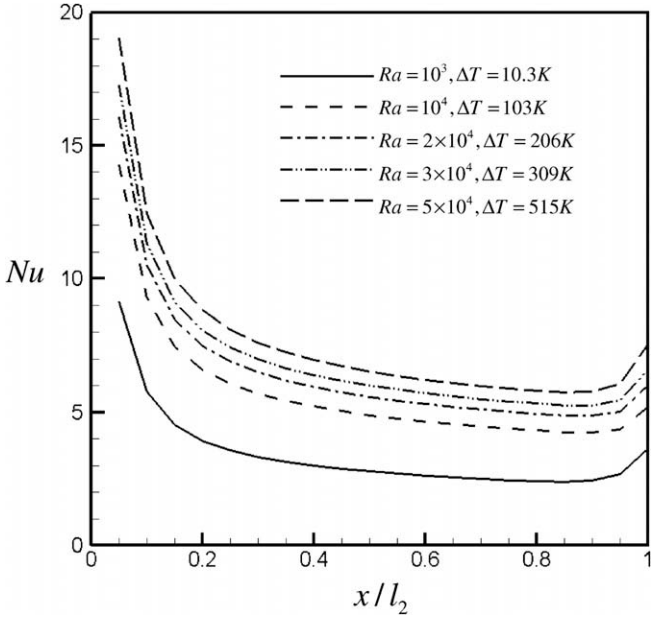

Fig. 9. Comparisons of the local Nusselt numbers on the heat surface for different Rayleigh numbers ($l_1/l_2 = 19$).

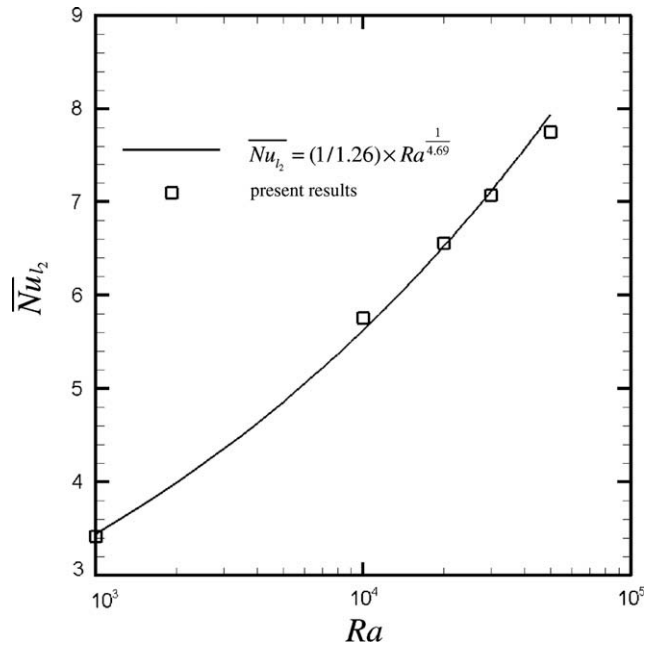

Fig. 10. Comparisons of the correlation equation and the present results ($l_1/l_2 = 19$).

1. Under a low temperature difference condition, the results obtained by the Bossinesq assumption and the present work are in good agreement.
2. Under a high temperature difference condition, the results obtained by the present work are reasonable.
3. The pressure at the inside of outlet is higher than that at the outside of the outlet.
4. Non-reflecting conditions are suitable for the boundary conditions at the inlet and outlet of the channel.
5. Two correlation equations which separately correlate the average Nusselt number to the Rayleigh number and the length of channel are proposed.

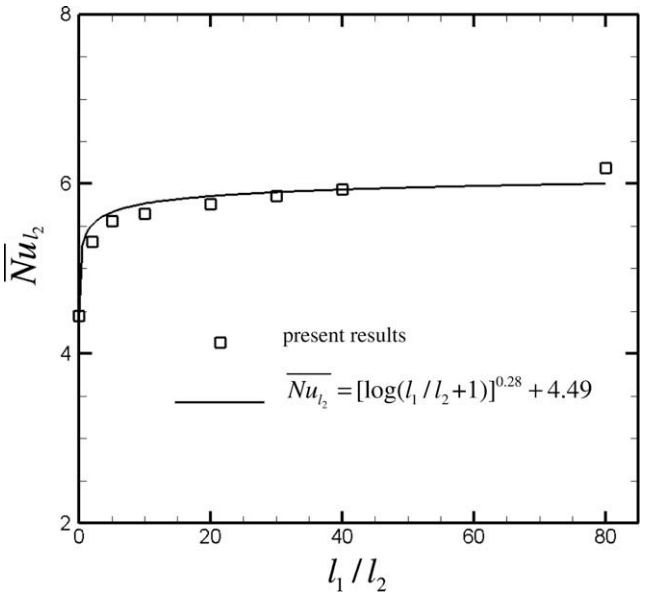

Fig. 11. The variations of average Nusselt number $\overline{Nu}_{l_2}$ with different ratios of l_1/l_2 ($Ra = 10^4$).

Acknowledgements

The authors gratefully acknowledge the support of the Natural Science Council, Taiwan, ROC under Contact NSC96-2221-E-009-059 and National Center for High-Performance Computing of Taiwan, ROC.

References

[1] P.H. Oosthuzien, A numerical study of laminar free convective flow through a vertical open partially heated plane duct, ASME HTD 32 (1984) 41–48.
[2] D. Naylor, J.M. Floryan, J.D. Tarasuk, A numerical study of developing free convection between vertical parallel plates, Trans. J. Heat Mass Transfer ASME 113 (1991) 620–626.
[3] D.A. Hall, G.C. Vliet, T.L. Bergman, Natural convection cooling of vertical rectangular channel in air considering radiation wall conduction, J. Electronic Packaging Trans. ASME 121 (1999) 75–84.
[4] W.S. Fu, C.P. Huang, Effects of a vibrational heat surface on natural convection in a vertical channel flow, Int. J. Heat Mass Transfer 49 (2006) 1340–1349.
[5] J.M. Floryan, M. Novak, Free convection heat transfer in multiple vertical channels, Int. J. Heat Fluid Flow 16 (1995) 245–253.
[6] J.R. Dyer, The development of laminar natural-convective flow in a vertical uniform heat flux duct, Int. J. Heat Mass Transfer 18 (1975) 1455–1465.
[7] D. Gilles, F. Alberto, Laminar natural convection in a vertical isothermal channel with symmetric surface-mounted rectangular ribs, Int. J. Heat Mass Transfer 23 (2002) 519–529.
[8] S.A.M. Said, M.A. Habib, H.M. Badr, S. Anwar, Numerical investigation of natural convection inside an inclined parallel-walled channel, Int. J. Numer. Methods Fluids 49 (2005) 569–582.
[9] D.D. Gray, A. Giorgini, The validity of the Boussinesq approximation for liquids and gases, Int. J. Heat Mass Transfer 19 (1976) 545–551.
[10] W.R. Briley, H. McDonald, S.J. Shamroth, At low Mach number Euler formulation and application to time iterative LBI schemes, AIAA 21 (10) (1983) 1467–1469.
[11] E. Turkel, Preconditioned methods for solving the incompressible and low speed compressible equations, J. Comput. Phys. 72 (1987) 277–298.
[12] D. Choi, C.L. Merkel, Application of time-iterative schemes to incompressible flow, AIAA 25 (6) (1985) 1518–1524.
[13] D. Choi, C.L. Merkel, The application of preconditioning in viscous flows, J. Comput. Phys. 105 (1993) 207–223.
[14] P.L. Roe, Approximation Riemann solver, parameter vectors, and difference schemes, J. Comput. Phys. 43 (1981) 357–372.
[15] J.M. Weiss, W.A. Simth, Preconditioning applied to variable and constants density flows, AIAA 33 (1995) 2050–2056.
[16] D.H. Rudy, J.C. Strikwerda, A nonreflecting outflow boundary condition for subsonic Navier–Stokes calculations, J. Comput. Phys. 36 (1980) 55–70.
[17] T.J. Poinsot, S.K. Lele, Boundary conditions for Navier–Stokes, J. Comput. Phys. 101 (1992) 104–129.
[18] H. Paillere, C. Viozat, A. Kumbaro, I. Toumi, Comparison of low Mach number models for natural convection problems, Heat Mass Transfer 36 (2000) 567–573.
[19] S. Yamamoto, D. Niiyama, R.S. Beyong, A numerical method for natural convection and heat conduction around and in a horizontal circular pipe, Int. J. Heat Mass Transfer 47 (2004) 5781–5792.
[20] J. Dennis, P. Thomas, B. Pieter, Recent Enhancements to OVERFLOW, Aerospace Sciences Meeting and Exhibit, 35th, Reno, NV, 1997.
[21] S.W. Churchill, H.H.S. Chu, Correlating equations for laminar and turbulent free convection from a vertical plate, Int. J. Heat Mass Transfer 18 (1975) 1323–1329.
[23] X. Xu, J.S. Lee, R.H. Pletcher, A compressible finite volume formulation for large eddy simulation of turbulent pipe flows at low Mach number in Cartesian coordinates, J. Comput. Phys. 203 (2005) 22–48.
[24] E. Lenormand, P. Saguat, L.T. Phuoc, Large eddy simulation of subsonic and supersonic channel flow at moderate Reynolds number, Int. J. Numer. Methods Fluids 32 (2000) 369–406.